

# Kinematic Edges with Flavor Splitting and Mixing

Iftah Galon<sup>1</sup> and Yael Shadmi<sup>1,2</sup>

<sup>1</sup>*Physics Department, Technion—Israel Institute of Technology, Haifa 32000, Israel*

<sup>2</sup>*Kavli Institute for Theoretical Physics,  
University of California, Santa Barbara, CA 93106*

## Abstract

The kinematic edges of invariant mass distributions provide an important tool for the possible measurements of superpartner masses in supersymmetric models with a neutralino LSP. We examine the effect of lepton flavor dependence on the kinematic endpoints of the di-lepton invariant mass distribution, with the leptons being electrons and muons. In the presence of slepton mass splitting and mixing, each of these distributions exhibits multiple edges, which are likely to be close. Furthermore, flavor subtraction, which is usually employed to eliminate backgrounds, dilutes the signal. We propose to extract the endpoints from the flavor-added distribution, which is insensitive to the slepton mixing. We also discuss the extraction of the slepton flavor parameters in such scenarios. To demonstrate our results, we use an example with a small slepton mass splitting of 3 GeV leading to a 6 GeV edge splitting, at both small mixing and large mixing.

PACS numbers: 11.30.Pb, 12.60.Jv, 14.80.Ly

## I. INTRODUCTION

Kinematic edges provide one of the main tools for extracting superpartner masses [1–8]. If supersymmetry, or other types of new physics, gives rise to events with cascade decays ending in a final state with invisible massive particles, then the events cannot be fully reconstructed, but various invariant-mass distributions exhibit edges whose locations depend on the superpartner masses. Given sufficient measurements of these edges, the masses can in principle be inferred [2].

The best studied kinematic edge is the endpoint in the invariant-mass distribution of opposite sign (OS) electrons and muons from the decay of a heavy neutralino  $\tilde{\chi}_2^0$  to a slepton  $\tilde{l}$ , followed by the subsequent slepton decay to the lightest neutralino  $\chi_1^0$ ,

$$\tilde{\chi}_2^0 \rightarrow \tilde{l}^\pm l_j^\mp \rightarrow \chi_1^0 l_j^\mp l_i^\pm. \quad (1)$$

The endpoint in this case depends on the neutralino and slepton masses through,

$$m_{ll}^2|_{\text{endpoint}} = \frac{(m_{\tilde{\chi}_2^0}^2 - m_{\tilde{l}}^2)(m_{\tilde{l}}^2 - m_{\chi_1^0}^2)}{m_{\tilde{l}}^2}. \quad (2)$$

Most studies of kinematic edges have assumed universal slepton masses, such that the selectron and smuon are degenerate with no flavor mixing. The leptons  $l_i$  and  $l_j$  in Eq. (1) are then either both electrons or both muons, and each of the same-flavor distributions exhibits a single endpoint: the  $e^\pm e^\mp$  ( $\mu^\pm \mu^\mp$ ) distribution is only sensitive to the selectron (smuon) mass. Furthermore, since the selectron and smuon are degenerate, the two endpoints coincide. These features have been used to eliminate backgrounds from uncorrelated leptons by considering the flavor-subtracted invariant mass distribution [1]

$$N_{e^+e^-} + N_{\mu^+\mu^-} - N_{e^\pm\mu^\mp}. \quad (3)$$

Scalar masses, however, need not be universal. Many examples of models with non-universal slepton masses are known (see for example [9–13]). The collider signatures of flavor-violating models have been discussed in [14–32]. At low-energies, such models generically give rise to slepton mass splittings *and* some degree of slepton flavor mixing. The reason is that theories that predict different slepton masses typically involve some new slepton quantum number, which determines the slepton masses. There is then some new slepton interaction basis in addition to the flavor basis, and the slepton masses are not necessarily diagonal in the flavor basis.

In the presence of both mass-splitting and mixings, each di-lepton invariant mass distribution, with  $l = e, \mu$ , exhibits two or more edges, associated with the different slepton states. Since the selectron-smuon mass splitting is likely to be small, the corresponding edges may be quite close. Compared to the usual scenario of universal slepton masses, the edge structure in this case is therefore less sharp. Furthermore, the same multiple edges appear in the flavor-subtracted distribution of Eq. (3). While this distribution still eliminates the background, it dilutes the signal as well, since the signal contributes to both the same-flavor and different-flavor decays.

The observation of kinematic edges in the presence of flavor mixing and splitting is thus more challenging. Even if an edge structure is observed, one would like to determine whether it is a single edge or a multiple edge, corresponding to two or more new particles with small

mass splittings. Finally, if multiple edges are observed, one would like to extract the flavor parameters from them. A measurement of these parameters may provide information both on the origin of the new physics, such as the mediation mechanism of supersymmetry breaking, and on the underlying theory of flavor.

In this paper, we study these questions using a toy model in which the lightest two sleptons are selectron-smuon mixtures. Since we are mainly interested in the ability to resolve a small edge splitting, we take the mass splitting to be roughly 3 GeV, leading to edges that are 6 GeV apart, and consider both small mixing and large mixing. The small mixing and large mixing cases are somewhat complimentary. In the former, it should probably be possible to observe the edges in the  $ee$  and  $\mu\mu$  distributions, since each one of them is dominated by a single edge. Indeed, the zero mixing case was studied in [33], where it was argued that the slepton mass splitting can be measured down to  $\Delta m_{\tilde{l}}/m_{\tilde{l}} \sim 10^{-4}$  (where  $\Delta m_{\tilde{l}}$  is the slepton mass splitting) in a 14 TeV LHC with  $30\text{fb}^{-1}$  integrated luminosity<sup>1</sup>. If the existence of different edge locations in the  $ee$  and  $\mu\mu$  distributions can be established, it would signal flavor dependence and provide motivation for looking for flavor mixing in the  $e\mu$  distribution. On the other hand, for large mixing, the edges in the same-flavor distributions would be harder to measure, but the  $e\mu$  distribution should exhibit some edge structure, which would indicate flavor mixing, and provide motivation for looking for edge splitting. In either case, as explained above, the precise determination of the edges would be non-trivial, because the edges are “divided” between the four distributions  $N_{l_i^+ l_j^-}$  with  $l_i, l_j = e, \mu$ .

To overcome this problem, we propose to consider the flavor-*added* distribution

$$N_{e^+e^-} + N_{\mu^+\mu^-} + N_{e^+\mu^-} + N_{e^-\mu^+}. \quad (4)$$

This is useful because: a. the edge locations are identical in all the four distributions appearing in Eq. (4) since they only depend on the slepton masses, b. the mixing, which affects each of the individual flavor distributions drops out of the flavor added distribution, and c. if a small edge splitting is the result of a small mass splitting, the two sleptons make roughly equal contributions to the flavor added distribution. While the flavor added-distribution Eq. (4) does not get rid of the background, it does not dilute the signal contributing to the edges, and could therefore exhibit a clearer edge structure than each of the separate flavor combinations. Once the edge locations are measured from Eq. (4), one can proceed to determine the mixing from the separate invariant mass-distributions  $N_{l_i^+ l_j^-}$ .

In order to see the effect of flavor dependence on kinematic edges, it is useful to compare the edge structures with flavor-dependence and without it. We therefore chose as our toy model the SU3 benchmark point [34] for which the selectron-smuon kinematic edge was carefully studied, and deformed it slightly by introducing a small selectron-smuon mass splitting and mixing by hand<sup>2</sup>.

Throughout our discussion, we assume that the slepton widths are much smaller than the mass splitting, so that slepton flavor oscillations can be neglected [14]. The effect of such oscillation on the edge structure is examined in [37].

The outline of this paper is as follows. In Sec. II we discuss the locations of the edges,

---

<sup>1</sup> This conclusion depends however on the values of the slepton masses relative to the neutralino masses [33] (see discussion in Section II).

<sup>2</sup> The SU3 benchmark point may be ruled out already by ATLAS [35] and CMS [36], but we are only interested in it as a toy example for assessing the effects of flavor dependence on the dilepton edge.

and the relative numbers of different flavor lepton pairs. In Sec. III we present the di-lepton invariant mass distributions for our toy model, and extract the end-points from the flavor-added distribution. We discuss the extraction of the remaining flavor parameters in Sec. IV. The spectrum of our toy model is given in Appendix A and the fitting functions we use in Appendix B.

## II. THE DI-LEPTON INVARIANT MASS DISTRIBUTIONS WITH MASS SPLITTING AND MIXING

We consider models in which two of the lightest sleptons, (typically the superpartners of the Right-Handed leptons) are selectron-smuon combinations, with

$$\begin{aligned}\tilde{l}_1 &= \cos \theta \tilde{e} - \sin \theta \tilde{\mu} \\ \tilde{l}_2 &= \sin \theta \tilde{e} + \cos \theta \tilde{\mu},\end{aligned}\tag{5}$$

with masses

$$m_{\tilde{l}_1} = m_{\tilde{l}}, \quad m_{\tilde{l}_2} = m_{\tilde{l}} + \Delta m_{\tilde{l}}.\tag{6}$$

We also assume that these slepton masses are between the two lightest neutralino masses, so that some of the heavier neutralinos  $\tilde{\chi}_2$  decay via Eq. (1). Neutralino decays via slepton  $i$  result in a di-lepton mass distribution which ends at

$$m_{ll}^2|_{edge,i} = \frac{(m_{\tilde{\chi}_2^0}^2 - m_{\tilde{l}_i}^2)(m_{\tilde{l}_i}^2 - m_{\tilde{\chi}_1^0}^2)}{m_{\tilde{l}_i}^2}.\tag{7}$$

For small slepton mass splitting, the difference between the endpoints can be approximated by [33]

$$\Delta m_{ll} = m_{ll}|_{edge,2} - m_{ll}|_{edge,1} \sim \frac{m_{ll}}{m_{\tilde{l}}} \frac{m_{\tilde{\chi}_2^0}^2 m_{\tilde{\chi}_1^0}^2 - m_{\tilde{l}}^4}{(m_{\tilde{\chi}_2^0}^2 - m_{\tilde{l}}^2)(m_{\tilde{l}}^2 - m_{\tilde{\chi}_1^0}^2)} \Delta m_{\tilde{l}}.\tag{8}$$

When the slepton mass  $m_{\tilde{l}}$  coincides with the geometric mean of the neutralino masses, the edge splitting vanishes<sup>3</sup>. This has an important effect on the ability to resolve different endpoints. For fixed neutralino masses, it would be easiest to observe the decay Eq. (1) for a slepton that is close to the geometric mean of the two neutralino masses, since then the phase space available for the two emitted leptons is large, so that the leptons are relatively hard. However, for such slepton masses, the edge splitting would be smaller than the slepton mass splitting. On the other hand, for slepton masses far from this geometric mean, the edge splitting can be larger than the slepton mass splittings, but since the sleptons are closer to one of the neutralinos, the phase space left for either the first or the second emitted leptons is diminished, so that this lepton is softer and therefore harder to detect.

Indeed, for the SU3 benchmark point, which was chosen partly in order to study kinematic edges assuming selectron-smuon universality, the slepton mass was taken to be 157 GeV,

---

<sup>3</sup> The reason is that the maximum of the edge Eq. (7) as a function of the slepton mass occurs at  $m_{\tilde{l}}^2 = m_{\tilde{\chi}_1^0} m_{\tilde{\chi}_2^0}$ , so around this point the sensitivity of the edge location to the precise value of the slepton mass is small (see Fig. 1).

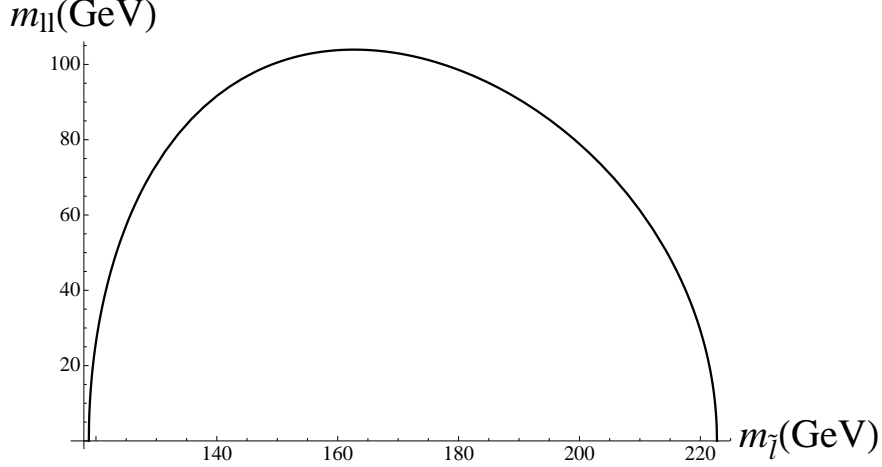


FIG. 1: The endpoint location,  $m_{ll}|_{\text{edge}}$ , as a function of the slepton mass,  $m_{\tilde{l}}$ , with the neutralino masses kept fixed at their SU3 values of  $m_{\chi_2^0} = 222$  GeV and  $m_{\chi_1^0} = 118$  GeV.

very close to  $\sqrt{m_{\chi_2^0} m_{\chi_1^0}} \sim 163$  GeV [34]. Around this mass, a small splitting between the sleptons could go unobserved in the edge structure. For example, for slepton masses varying between 140 GeV and 185 GeV the edge splitting is at most 5 GeV as can be seen in Fig. 1.

The numbers of events in the different di-lepton flavor contributions are related by,

$$\begin{aligned} \frac{N(e^\pm \mu^\mp)}{N(e^+ e^-)} &= \frac{2(1+R) \cos^2 \theta \sin^2 \theta}{\cos^4 \theta + R \sin^4 \theta} \\ \frac{N(\mu^+ \mu^-)}{N(e^+ e^-)} &= \frac{R \cos^4 \theta + \sin^4 \theta}{\cos^4 \theta + R \sin^4 \theta}, \end{aligned} \quad (9)$$

where  $R$  is the ratio of phase space factors in decays involving different sleptons:

$$R \equiv \left( \frac{m_{\chi_2^0}^2 - m_{\tilde{l}_2}^2}{m_{\chi_2^0}^2 - m_{\tilde{l}_1}^2} \right)^2, \quad (10)$$

which is close to one for near-degenerate sleptons.

As mentioned in the Introduction, in the presence of mixing, the flavor subtracted distribution dilutes the signal. In Figure 2 we plot the ratio of the flavor-subtracted distribution Eq. (3) to the total distribution,

$$\begin{aligned} \eta &\equiv \frac{N(e^+ e^-)/\beta + \beta N(\mu^+ \mu^-) - N(e^\pm \mu^\mp)}{N(e^+ e^-)/\beta + \beta N(\mu^+ \mu^-) + N(e^\pm \mu^\mp)} \\ &= 1 - \frac{\beta \sin^2 2\theta}{(\beta + \sin^2 \theta (1 - \beta))^2 + \left( \frac{1 - \beta^2}{1 + R} \right) \cos 2\theta} \end{aligned} \quad (11)$$

as a function of the mixing for different values of  $R$ . Here  $\beta$  is the ratio of electron efficiency to muon efficiency in the experiment. The weak  $R$ -dependence in Figure 2 is a result of the fact that we took the ATLAS value,  $\beta = 0.86$  which is close to one. As expected,  $\eta$  vanishes for maximal mixing, but even for a mixing of  $\sin \theta \simeq 0.3$   $\eta$  drops to  $\sim 0.6$ .

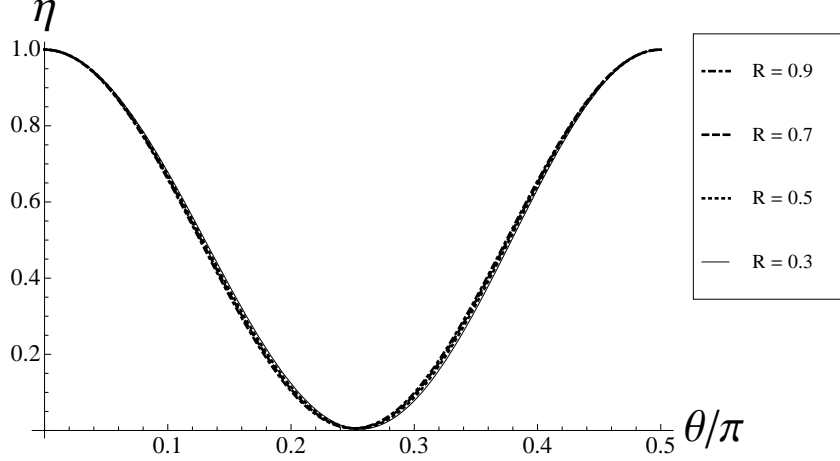


FIG. 2:  $\eta$  (of Eq. (11)) as a function of the mixing angle  $\theta$ , for several values of  $R = 0.3, 0.5, 0.7, 0.9$ , with  $\beta = 0.86$ .

### III. TOY MODELS AND RESULTS

#### A. Model parameters and simulation

As mentioned above, we use two toy models based on the SU3 benchmark point, and modify the right-handed selectron and smuon states. The two lightest neutralino masses are 118 GeV and 222 GeV. The remaining masses are given in Table II of Appendix A. Based on the discussion of the previous section, we want the slepton masses to be sufficiently far from the geometric mean of the two neutralino masses  $\sim 160$  GeV, so that the effect of a small slepton mass splitting is not suppressed in the edge splitting, but at the same time, not too close to the neutralino masses, so that the resulting leptons are not too soft. We also exclude slepton masses in the ranges  $135 \text{ GeV} \leq m_{\tilde{l}} \leq 147 \text{ GeV}$  and  $180 \text{ GeV} \leq m_{\tilde{l}} \leq 196 \text{ GeV}$  in order for the edge to be separated by at least 7 GeV from the  $Z$  resonance.

Bounds on lepton flavor violation limit the possible mass splitting and mixing. For small mass splitting, the constrained quantity is essentially

$$\delta_{12}^R \sim \frac{(\Delta m_{\tilde{l}})^2}{m_{\tilde{l}}^2} \sin \theta. \quad (12)$$

The experimental constraints on  $\mu \rightarrow e\gamma$  [38] imply, using [39, 40],  $\delta_{12}^R \leq 0.09$ .

Given the considerations above, we choose the slepton masses to be  $m_{\tilde{l}_1} = 131 \text{ GeV}$ , and  $m_{\tilde{l}_2} = 133.8 \text{ GeV}$ . With these masses, the mixing is not constrained. The resulting endpoint locations are,

$$\begin{aligned} m_{ll} (m_{\tilde{l}_1} = 131 \text{ GeV})|_{edge} &= 75.9 \text{ GeV} \\ m_{ll} (m_{\tilde{l}_2} = 133.8 \text{ GeV})|_{edge} &= 81.9 \text{ GeV} \end{aligned} \quad (13)$$

with  $\Delta m_{ll} \sim 6 \text{ GeV}$ . The two models we study differ only in the mixing angle. One has small mixing with  $\sin^2 \theta \simeq 0.9$ , and the other has large mixing with  $\sin^2 \theta \simeq 0.4$ .

Since we are interested in a comparison of the flavor-dependent di-lepton edges to the

SU3 study, which assumed 14 TeV center-of-mass energy, we generate  $1.5 \cdot 10^5$  SUSY strong production events and  $6 \cdot 10^6$   $t\bar{t}$  SM events, corresponding to  $10 \text{ fb}^{-1}$  at a 14 TeV LHC, and use the same cuts as those used in the SU3 study [34]:

1. Exactly two isolated opposite sign leptons ( $e, \mu$ ) with  $p_T > 10 \text{ GeV}$  and  $|\eta| < 2.5$ .
2. At least four jets with  $p_T > 50 \text{ GeV}$ , at least one of which has  $p_T > 100 \text{ GeV}$ .
3.  $\cancel{E}_T > 100 \text{ GeV}$  and  $\cancel{E}_T > 0.2 M_{\text{effective}}$ .
4. Transverse Sphericity  $S_T > 0.2$ .

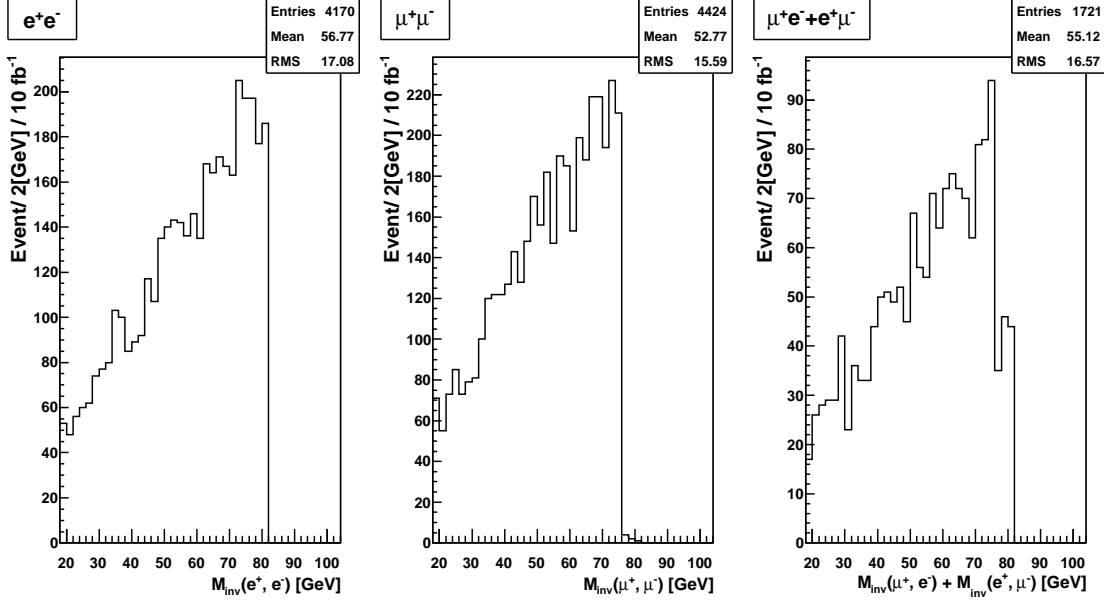
Based on the SU3 analysis, other types of SM backgrounds are omitted as they become irrelevant after the cuts. We note that less than 5% of the signal events survive the experimental cuts.

The spectrum for the SU3 model is calculated using SPICE [41], which is based on SoftSUSY [42] and SUSYHIT [43]. We then modify the selectron and smuon masses, and introduce selectron-smuon mixing by hand at low energies. To simulate events we use MadGraph-MadEvent (MGME) [44], with FeynRules [45]. The resulting events are decayed using BRIDGE [46] and put back into MGME’s Pythia-PGS package [47–49] which includes hadronization and initial and final state radiation. We use ROOT [50] to handle the results, via MGME’s ExROOTAnalysis package [51].

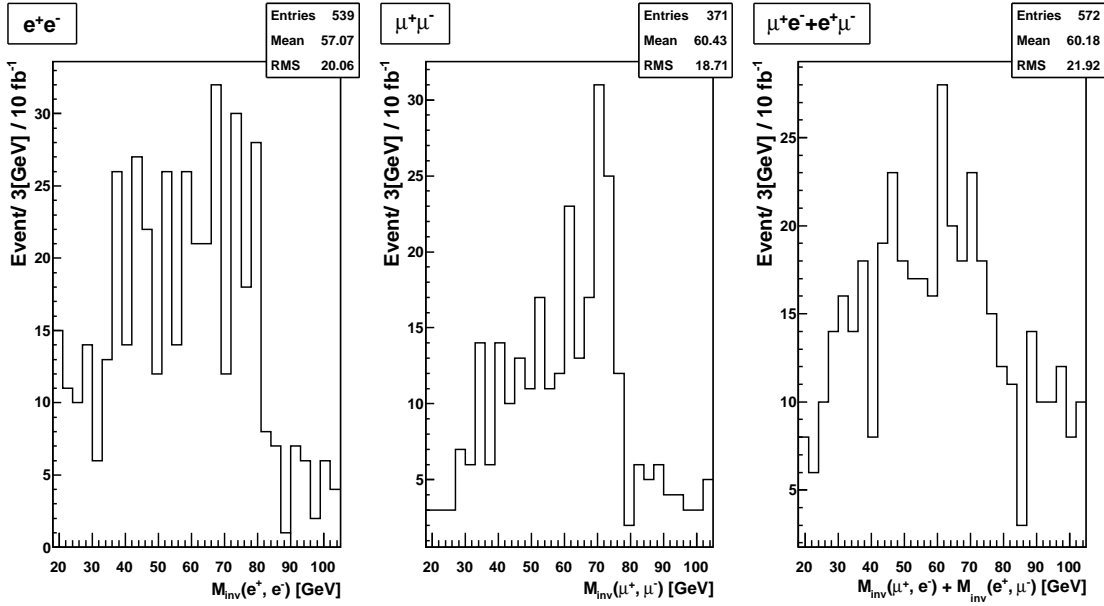
## B. Resolving the Edges Using Flavor Addition

The di-lepton invariant mass distributions for the different flavor combinations for small mixing and for large mixing are shown in Figure 3 and Figure 4 respectively. In each case, the truth distribution (Fig. 3(a), Fig. 4(a)) contains the signal only, that is, the di-leptons coming from the decay chain Eq. (1) at the generator level, with no background from either supersymmetric events or from top production. The “experimental” distributions (Fig. 3(b), Fig. 4(b)) contain both the signal and the background, after the PGS detector simulation. Note that the background consists of all the possible lepton pairs from the supersymmetric events, including leptons from decays of charginos,  $Z$  etc, as well as from SM  $t\bar{t}$  production. As expected, for small mixing, the  $ee$  and  $\mu\mu$  distributions are dominated by a single slepton, and therefore exhibit a single edge to a good approximation. This edge can be easily seen in the corresponding experimental distributions. In contrast, all the remaining truth distributions exhibit a double edge structure, which translates to a much fuzzier structure once background and detector effects are taken into account.

In order to obtain clearer edges we therefore exploit the fact that the edge locations coincide in these different distributions, and consider the flavor-added dilepton invariant mass distribution  $N_{l+l-}$  with  $l = e, \mu$ . Using Eq. (9), it is easy to see that this distribution is independent of the mixing, with the  $\tilde{l}_1, \tilde{l}_2$  contributions differing by the phase space ratio  $R$ . In Fig. 5, we plot the flavor-added “experimental” invariant-mass distributions. As above, these contain both the signal and background, with the background consisting of all the possible lepton pairs from the supersymmetric events, including leptons from decays of charginos,  $Z$  etc, as well as from SM  $t\bar{t}$  production. Indeed, one can observe two distinct edges. To determine the locations of these edges, we fit the distribution with two triangles over a constant background, convoluted with Gaussian noise (see Eq. (B4) of Appendix B).



(a) Truth distributions (2 GeV per bin)

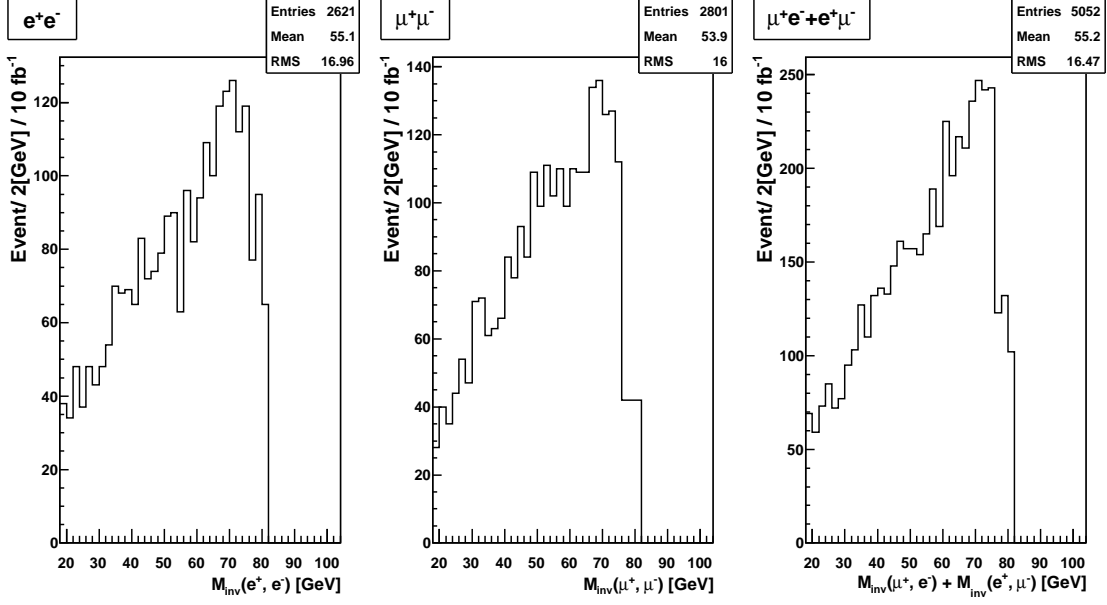


(b) "Experimental" distributions (3 GeV per bin)

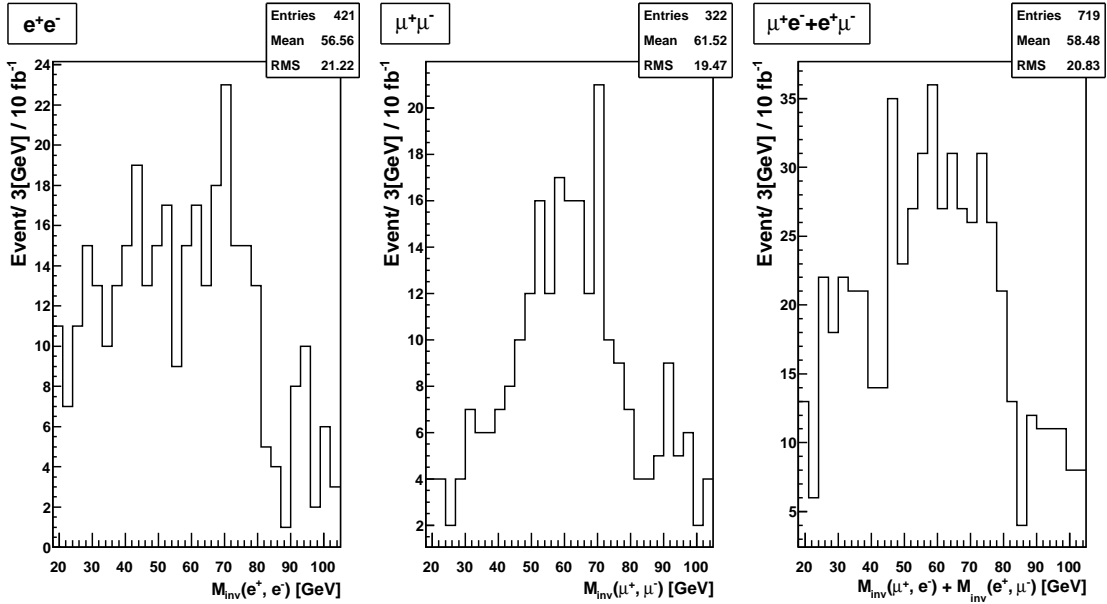
FIG. 3: The opposite-sign-di-lepton invariant mass distributions from truth—signal only before detector simulation (top), and “experimental”—including background and detector simulation (bottom) for Model 1—small mixing.

Since the edges are clearly very close, we can try first setting  $R = 1$ , for which the two slepton contributions are equal. This is a good approximation if the small edge splitting is the result of a small slepton mass splitting. Expanding in  $\Delta m_{\tilde{l}}$ , it is easy to see that the deviation of  $R$  from 1 affects the distribution only at  $\mathcal{O}(\Delta m_{\tilde{l}}^2)$ . However, as explained in Sec. II, a small edge splitting does not necessarily imply a small mass splitting. In this case, taking  $R = 1$  would give a poor fit. We will return to this case in the next section.





(a) Truth distributions 2 GeV per bin

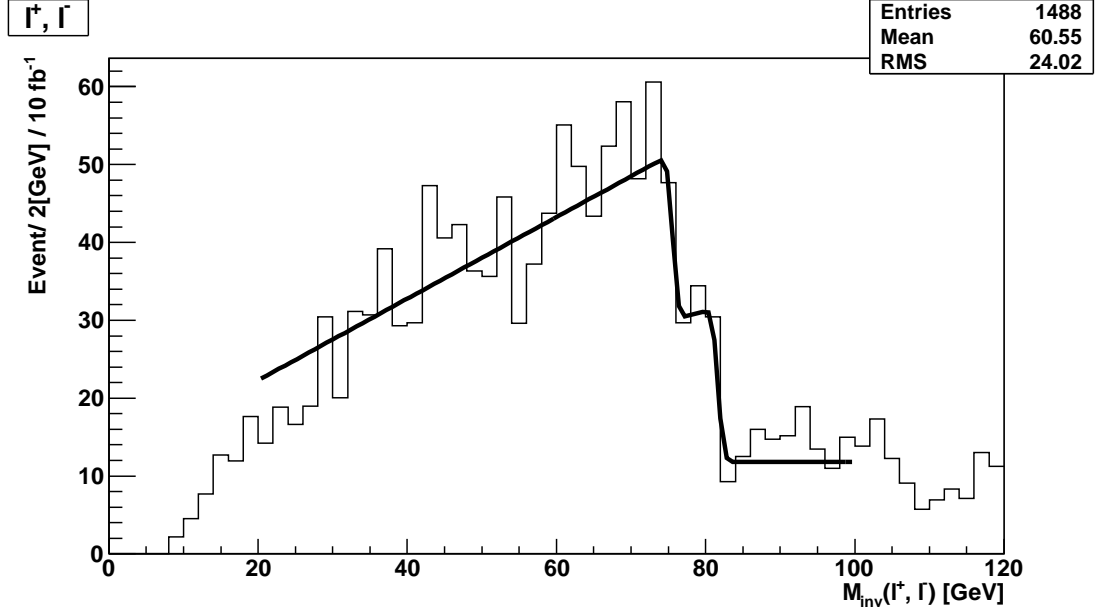


(b) "Experimental" distributions 3 GeV per bin

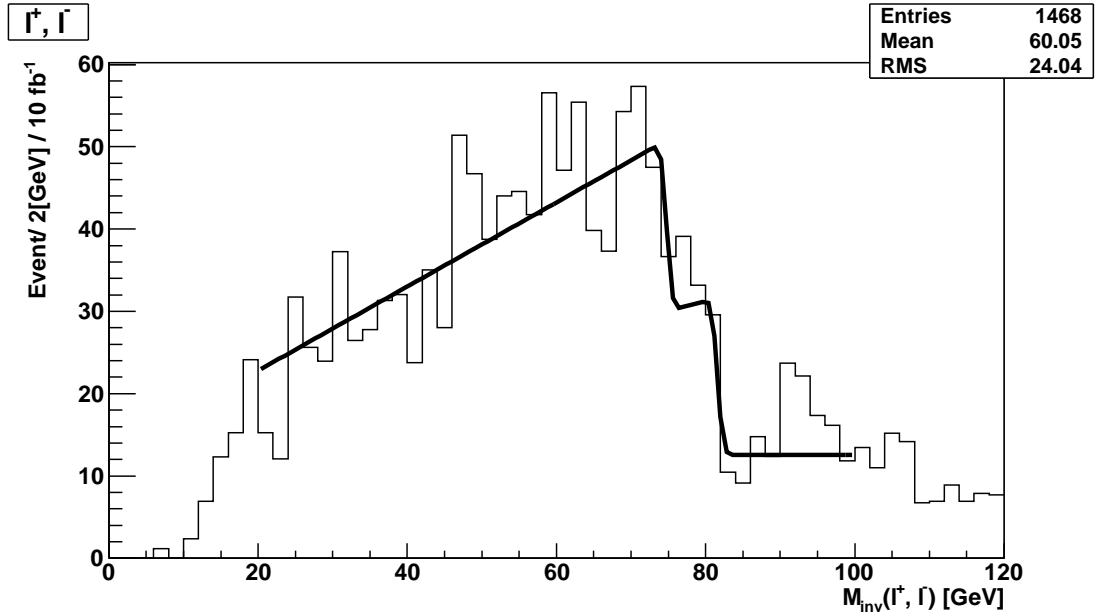
FIG. 4: The opposite-sign-di-lepton invariant mass distributions from truth—signal only before detector simulation (top), and “experimental”—including background and detector simulation (bottom) for Model 2—large mixing.

The four fit parameters are then the two endpoints, the constant background, and the total number of events<sup>4</sup> and we find the endpoints at 75.6 GeV and 81.7 GeV (for the small mixing

<sup>4</sup> The Gaussian noise parameter,  $\sigma = 0.57$ , is extracted from the opposite-sign-same-flavor di-lepton  $Z$  resonance, which gives a reasonable approximation since it is close to the endpoint.



(a) Model 1–small mixing



(b) Model 2–large mixing

FIG. 5: The opposite-sign-di-lepton flavor-added “experimental” invariant-mass distribution,  $N_{e^+e^-} + N_{\mu^+\mu^-} + N_{e^\pm\mu^\mp}$ , for the two models at 2 GeV per bin.

model) and at 74.8 GeV and 81.6 GeV (for the large mixing model), indicating that the two different edges can be resolved in this case.

The ability to resolve the edges depends of course on the binning, which is determined in turn by the available statistics. For coarser bins, of width larger than 6 GeV, only a single edge can possibly be detected for our choice of model parameters. Conversely with much higher statistics and smaller bin sizes one can probably observe a sharper double-edge structure. Here we wanted to focus on the trickiest scenario with the edge separation just

slightly above the statistically-significant bin size.

We note that before any fit is done, each of the distributions is scaled by the the proper power of  $\beta$  (the ratio of electron to muon efficiencies). We “measure” the relevant efficiencies in our sample to be roughly 0.47 for electrons, and 0.4 for muons, with  $\beta \sim 1.18$ . These low efficiencies are the result of the large number of jets in the events, combined with the requirement of isolated leptons. It is quite possible that the endpoint resolution might be improved with a different set of cuts. Thus for example, the decay chain (1) does not require gluino pair production. If it originates from squark pair production, it could be accompanied by only two jets. If only neutralinos, charginos and sleptons can be produced at the LHC the event selection would be completely different. With fewer jets in the final state the efficiency for leptons would be much higher.

Equipped with the results for the endpoints from the flavor-added distribution, one can return to the individual flavor combinations of Figs. 3(b) and 4(b), and extract additional information, starting with the mixing. We will discuss this in Sec. IV. If one has reason to believe that the individual distributions of Figs. 3(b) and 4(b) exhibit double edges, one can of course try to simultaneously fit them with a double triangle. This fit, however, is quite sensitive to initial conditions since it involves six parameters: the total number of events, the two endpoints,  $R$ , the mixing  $\sin\theta$  and the constant background.

As explained above, our anchor model was the SU3 benchmark point, with degenerate selectron and smuon masses at 156 GeV [34]. The endpoint in this case was obtained using flavor subtraction at  $m_{ll}|_{\text{endpoint}} = 99.7 \pm 1.4|_{\text{stat}} \pm 0.3|_{\text{sys}}$  GeV (the true value was 100.2 GeV). The SU3 analysis considered SUSY strong production cross-sections at next to leading order  $\sigma^{NLO} = 27.68(\text{pb})$  for which 500K events were produced (the results were then normalized to  $1\text{fb}^{-1}$ ). Our analysis includes a more modest data sample with only leading order cross-sections of  $\sigma^{LO} \sim 15(\text{pb})$  (we give our results for  $10\text{fb}^{-1}$ ). The number of produced events and the obtained signal samples are however in proportion. Our background estimation was rather lenient and relied on the SU3 results which indicated that the only significant contribution is from  $t\bar{t}$ . The most important ingredient of the detector simulation for our analysis is the electron and muon efficiencies. As explained above, these efficiencies were very low, because of the large number of jets in the events, with a larger efficiency for electrons<sup>5</sup>. Furthermore, the SU3 analysis used an optimized set of cuts in order to obtain the precise endpoint locations quoted above, which we have not attempted. Clearly then, a much better precision can be achieved for the model we discussed here. A careful estimate of the possible sensitivity to double edges is certainly beyond the scope of this paper (and our ability as theorists). Our main objective here is to examine whether edges can be detected at all in the presence of both splitting and mixing, and if that is the case, whether double edges can be resolved. As we saw above, for the models we considered here, with a  $\sim 6$  GeV edge splitting, the edge structure of the separate flavor distributions was hard to detect, but the flavor-added distribution indeed allowed for resolving the endpoints.

#### IV. UNDERSTANDING THE FLAVOR OF SLEPTONS

If an edge structure is discovered in the di-lepton invariant mass distribution, it would hint at new particles that couple to electrons and muons, such as the slepton(s) and neutralinos

---

<sup>5</sup> Our overall efficiency was roughly similar to the SU3 study [34].

of supersymmetry. The first “flavor question” one would be faced with then is whether there is a single “slepton” or multiple sleptons with similar masses. The observation of two different edges in  $N_{l_l l_j}$  would be a clear indication of the latter. However, this may not be possible if the two sleptons are almost degenerate, or, if their masses are close to  $\sqrt{m_{\chi_2^0} m_{\chi_1^0}}$  so that the edge splitting is suppressed as explained in Sec. II.

In this latter case, the appearance of  $R$  in Eq. (9) provides complementary information on the slepton masses, since it involves different combinations of the slepton and neutralino masses. As long as the slepton mass splitting is not too small, the different ratios in Eq. (9) may provide a measurement of  $R \neq 1$ , and therefore establish the existence of two slepton states with different couplings to electrons and muons.

As we argued in Sec. III, the flavor added distribution is very useful for measuring the endpoints, because it does not dilute the signal, and is independent of the mixing. Once the endpoints are measured from this distribution, one can turn to the individual flavor combinations and simultaneously fit them using Eq. (9) (see Appendix B 4) with the values found for the two endpoints as input. The fit depends on four parameters: the number of signal events,  $R$ , the mixing  $\sin \theta$  and the constant background. Performing this fit for our two toy models, we extract the mixing reasonably well, with  $\sin^2 \theta = 0.8$  (compared to the true value of 0.9) for the small mixing model, and  $\sin^2 \theta = 0.5$  (compared to 0.6) for the large mixing model. The results are collected in Table I.

(a) Model 1–small mixing				(b) Model 2 - large mixing			
Parameter	Truth	“Measured”	Error	Parameter	Truth	“Measured”	Error
$EP1$	75.86	75.57	0.76	$EP1$	75.86	74.75	0.39
$EP2$	81.87	81.68	0.55	$EP2$	81.87	81.61	0.60
$R$	0.95	1.19	0.13	$R$	0.95	1.79	0.69
$\sin^2 \theta$	0.91	0.79	0.02	$\sin^2 \theta$	0.585	0.534	0.043

TABLE I: Fit results for the endpoints and flavor parameters for Model 1–small mixing and Model 2–large mixing. The errors are only the fit errors.

With the value of  $R$  and the two endpoints measured, one has three different combinations of the two slepton masses and the two neutralino masses, and can therefore extract three relations between these soft masses.

## V. CONCLUSIONS

Existing tools for the measurement of superpartner masses often rely on the assumption of scalar mass degeneracy. Here we studied the effect of flavor dependence on the kinematic edges in the di-lepton mass distribution. It would be interesting to extend this study to distributions involving quarks as well.

If new physics is discovered at the LHC, one would eventually like to understand whether it exhibits any flavor dependence. Are the new states single states, with universal couplings to different standard model generations? Are they single states with generation-dependent couplings? Are there three copies of new states with different or equal masses and with different couplings to the standard model generations? In [9], these questions were studied for the case of supersymmetry with a meta-stable slepton, which allows for full reconstruction of

supersymmetric events. In this paper, we explored these questions in the more difficult scenario of supersymmetry with a neutralino LSP, focusing on the measurements of kinematic edges in di-lepton mass distributions. We discussed methods for resolving double edges, and for extracting the mixing. In particular, measurements of both the end-points and the relative rates of the  $ee$ ,  $\mu\mu$ , and  $e\mu$  distributions can yield complementary information on the slepton flavor parameters.

Finally, we note that we focused here on supersymmetric extensions of the standard model, assuming that the supersymmetric nature of the new particles is already established by other means. In fact, the invariant mass distributions of dileptons from cascade decays of new particles may provide important information on the spins of these new particles, and thus allow for distinguishing between various types of new physics, such as supersymmetry and extra dimensions [52]. As is well known, if the intermediate particles involved in the decay have nonzero spin, the resulting invariant mass distribution is no longer a triangle (see, e.g. [53] and references therein). The smeared double edge structure that we have discussed here could be hard to differentiate from a distribution arising in the case of, e.g., universal extra dimensions. Thus, the “inverse problem” [54] of distinguishing between different new physics scenarios is exacerbated by flavor dependence. It would be interesting to explore these questions further.

## VI. ACKNOWLEDGMENTS

We thank Y. Grossman, A. Harel, E. Kajomovitz, Y. Rozen and S. Tarem for useful discussions. We thank D. Cohen for computer support. We are grateful to J. Alwall, B. Fuks, M. Reece and especially J. Conway for answering many questions about MGME, FeynRules, BRIDGE and PGS. Y.S. thanks the KITP Santa Barbara where part of this work was completed. Research supported in part by the Israel Science Foundation (ISF) under grant No. 1155/07, by the United States-Israel Binational Science Foundation (BSF) under grant No. 2006071, and by the National Science Foundation under Grant No. PHY05-51164.

### Appendix A: The SU3 Spectrum

SU3 is an mSUGRA model defined by the following boundary conditions:

$$m_0 = 100 \text{ GeV} \quad m_{1/2} = 300 \text{ GeV} \quad A_0 = -300 \text{ GeV} \quad \tan \beta = 6 \quad \mu > 0. \quad (\text{A1})$$

The resulting spectrum appears in Table II.

Particles	Mass [GeV]	Particles	Mass [GeV]
$\tilde{\nu}_1$	216	$\tilde{\chi}_2^+$	477
$\tilde{\nu}_2$	217	$\tilde{\chi}_1^+$	222
$\tilde{\nu}_3$	217	$\tilde{g}$	718
$\tilde{\chi}_4^0$	477	$\tilde{l}_3$	151
$\tilde{\chi}_3^0$	462	$\tilde{l}_4$	231
$\tilde{\chi}_2^0$	222	$\tilde{l}_5$	231
$\tilde{\chi}_1^0$	118	$\tilde{l}_6$	232
$\tilde{u}^1$	451	$\tilde{d}^1$	602
$\tilde{u}^2$	643	$\tilde{d}^2$	639
$\tilde{u}^3$	643	$\tilde{d}^3$	642
$\tilde{u}^4$	664	$\tilde{d}^4$	642
$\tilde{u}^5$	664	$\tilde{d}^5$	668
$\tilde{u}^6$	664	$\tilde{d}^6$	668
$h^0$	110	$H^0$	513
$A^0$	512	$H^+$	518

TABLE II: Spectrum of the SU3 Model, calculated using SPICE.

## Appendix B: Functions Describing Triangular Distributions

### 1. A Single Triangle Function

For the triangle fit we use

$$T_1(x, [E, S]) = \begin{cases} 0 & x < 0 \\ 2 \left( \frac{S}{E^2} \right) x & 0 \leq x \leq E \\ 0 & x > E \end{cases} \quad (\text{B1})$$

Here  $E$  is the endpoint and  $S$  is the area of the triangle proportional to the total number of events in the distribution.

### 2. A Double Triangle Function

We describe the sum of two triangles based at zero with two different endpoints and slopes by:

$$T_2(x, [E_1, S_1, E_2, Ratio]) = T_1(x, [E_1, S_1]) + T_1(x, [E_2, S_2]) \quad (\text{B2})$$

where

$$S_2 = S_1 \times Ratio \quad (\text{B3})$$

and  $Ratio$  is the ratio of the triangle areas.

### 3. A Double Triangle Convolved With A Gaussian Function

To account for the noise in the measurement of particle momenta one must convolute the distributions with a Gaussian. The smearing parameter for our detector is measured from  $Z \rightarrow l^+l^-$  and is  $\sigma = 0.568$ . We use:

$$N_2T(x, [\sigma, E_1, S_1, E_2, Ratio]) = \frac{1}{\sqrt{2\pi}\sigma^2} \int_{-\infty}^{\infty} dx' e^{-\frac{(x-x')^2}{2\sigma^2}} T_2(x', [E_1, S_1, E_2, Ratio]) \quad (B4)$$

### 4. Simultaneous Fit Function

Our “measured” data set consists of the 3 di-lepton invariant mass distributions  $e^+e^-, \mu^+\mu^-, e^\pm\mu^\mp$ . To fit them simultaneously we use:

$$\text{Simultaneous}(x, [\sigma, E_1, E_2, \sin^2 \theta, R, S_{ee}, B_{ee}, B_{\mu\mu}]) = \begin{cases} f_{ee} & \text{for ee histogram} \\ f_{\mu\mu} & \text{for mumu histogram} \\ f_{e\mu} & \text{for emu histogram} \end{cases} \quad (B5)$$

here  $\sigma$  is the smearing parameter,  $E_1, E_2$  are the two endpoints,  $S_{ee}$  is the combined area of the two triangles in the  $ee$  distribution,  $B_{ll}$  is the constant background in the  $ll$  distribution. In addition,

$$\begin{aligned} f_{ee} &= N_2T(x, \left[ \sigma, E_1, S_{ee} \frac{\cos^4 \theta}{\cos^4 \theta + R \sin^4 \theta}, E_2, R \frac{\sin^4 \theta}{\cos^4 \theta} \right]) + B_{ee} \\ f_{\mu\mu} &= N_2T(x, \left[ \sigma, E_1, S_{\mu\mu} \frac{\sin^4 \theta}{\sin^4 \theta + R \cos^4 \theta}, E_2, R \frac{\cos^4 \theta}{\sin^4 \theta} \right]) + B_{\mu\mu} \\ f_{e\mu} &= N_2T(x, \left[ \sigma, E_1, S_{e\mu} \frac{1}{1+R}, E_2, R \right]) + B_{ee} + B_{\mu\mu} \end{aligned} \quad (B6)$$

where we have defined:

$$S_{\mu\mu} = S_{ee} \times \frac{\sin^4 \theta + R \cos^4 \theta}{\cos^4 \theta + R \sin^4 \theta} \quad (B7)$$

$$S_{e\mu} = S_{ee} \times 2 \frac{(1+R) \sin^2 \theta \cos^2 \theta}{\cos^4 \theta + R \sin^4 \theta} \quad (B8)$$

so that  $S_{\mu\mu} (S_{e\mu})$  is the total area of the two triangles in the  $\mu\mu (e\mu)$  distribution.

- 
- [1] I. Hinchliffe, F. Paige, M. Shapiro, J. Soderqvist, and W. Yao, “Precision SUSY measurements at CERN LHC,” *Phys.Rev.* **D55** (1997) 5520–5540, [arXiv:hep-ph/9610544](#) [hep-ph].
  - [2] I. Hinchliffe and F. Paige, “Measurements in gauge mediated SUSY breaking models at CERN LHC,” *Phys.Rev.* **D60** (1999) 095002, [arXiv:hep-ph/9812233](#) [hep-ph].

- [3] H. Bachacou, I. Hinchliffe, and F. E. Paige, “Measurements of masses in SUGRA models at CERN LHC,” *Phys.Rev.* **D62** (2000) 015009, [arXiv:hep-ph/9907518 \[hep-ph\]](#).
- [4] C. G. Lester, M. A. Parker, and . White, Martin J., “Determining SUSY model parameters and masses at the LHC using cross-sections, kinematic edges and other observables,” *JHEP* **0601** (2006) 080, [arXiv:hep-ph/0508143 \[hep-ph\]](#).
- [5] C. Lester, M. A. Parker, and . White, Martin J., “Three body kinematic endpoints in SUSY models with non-universal Higgs masses,” *JHEP* **0710** (2007) 051, [arXiv:hep-ph/0609298 \[hep-ph\]](#).
- [6] B. Gjelsten, . Miller, D.J., and P. Osland, “Measurement of SUSY masses via cascade decays for SPS 1a,” *JHEP* **0412** (2004) 003, [arXiv:hep-ph/0410303 \[hep-ph\]](#).
- [7] C. Autermann, B. Mura, C. Sander, H. Schettler, and P. Schleper, “Determination of supersymmetric masses using kinematic fits at the LHC,” [arXiv:0911.2607 \[hep-ph\]](#).
- [8] A. J. Barr, B. Gripaios, and C. G. Lester, “Weighing Wimps with Kinks at Colliders: Invisible Particle Mass Measurements from Endpoints,” *JHEP* **0802** (2008) 014, [arXiv:0711.4008 \[hep-ph\]](#).
- [9] J. L. Feng, C. G. Lester, Y. Nir, and Y. Shadmi, “The Standard Model and Supersymmetric Flavor Puzzles at the Large Hadron Collider,” *Phys.Rev.* **D77** (2008) 076002, [arXiv:0712.0674 \[hep-ph\]](#).
- [10] G. D. Kribs, E. Poppitz, and N. Weiner, “Flavor in supersymmetry with an extended R-symmetry,” *Phys. Rev.* **D78** (2008) 055010, [arXiv:0712.2039 \[hep-ph\]](#).
- [11] Y. Nomura and D. Stolarski, “Naturally Flavorful Supersymmetry at the LHC,” *Phys. Rev.* **D78** (2008) 095011, [arXiv:0808.1380 \[hep-ph\]](#).
- [12] Y. Shadmi and P. Z. Szabo, “Flavored Gauge-Mediation,” [arXiv:1103.0292 \[hep-ph\]](#).
- [13] C. Gross and G. Hiller, “Flavorful hybrid anomaly-gravity mediation,” [arXiv:1101.5352 \[hep-ph\]](#).
- [14] N. Arkani-Hamed, H.-C. Cheng, J. L. Feng, and L. J. Hall, “Probing Lepton Flavor Violation at Future Colliders,” *Phys. Rev. Lett.* **77** (1996) 1937–1940, [arXiv:hep-ph/9603431](#).
- [15] N. Arkani-Hamed, J. L. Feng, L. J. Hall, and H.-C. Cheng, “CP violation from slepton oscillations at the LHC and NLC,” *Nucl. Phys.* **B505** (1997) 3–39, [arXiv:hep-ph/9704205](#).
- [16] K. Agashe and M. Graesser, “Signals of supersymmetric lepton flavor violation at the LHC,” *Phys. Rev.* **D61** (2000) 075008, [arXiv:hep-ph/9904422](#).
- [17] J. Hisano, R. Kitano, and M. M. Nojiri, “Slepton oscillation at Large Hadron Collider,” *Phys. Rev.* **D65** (2002) 116002, [arXiv:hep-ph/0202129](#).
- [18] A. Bartl, K. Hidaka, K. Hohenwarter-Sodek, T. Kernreiter, W. Majerotto, *et al.*, “Test of lepton flavor violation at LHC,” *Eur.Phys.J.* **C46** (2006) 783–789, [arXiv:hep-ph/0510074 \[hep-ph\]](#).
- [19] R. Kitano, “A Clean Slepton Mixing Signal at the LHC,” *JHEP* **03** (2008) 023, [arXiv:0801.3486 \[hep-ph\]](#).
- [20] S. Kaneko, J. Sato, T. Shimomura, O. Vives, and M. Yamanaka, “Measuring Lepton Flavour Violation at LHC with Long-Lived Slepton in the Coannihilation Region,” *Phys. Rev.* **D78** (2008) 116013, [arXiv:0811.0703 \[hep-ph\]](#).
- [21] J. Hisano, M. M. Nojiri, and W. Sreethawong, “Discriminating Electroweak-ino Parameter Ordering at the LHC and Its Impact on LFV Studies,” *JHEP* **0906** (2009) 044, [arXiv:0812.4496 \[hep-ph\]](#).
- [22] J. Esteves, J. Romao, A. Villanova del Moral, M. Hirsch, J. Valle, *et al.*, “Flavour violation at the LHC: type-I versus type-II seesaw in minimal supergravity,” *JHEP* **0905** (2009) 003,



- arXiv:0903.1408 [hep-ph].
- [23] A. J. Buras, L. Calibbi, and P. Paradisi, “Slepton mass-splittings as a signal of LFV at the LHC,” *JHEP* **1006** (2010) 042, arXiv:0912.1309 [hep-ph].
  - [24] J. L. Feng, I. Galon, D. Sanford, Y. Shadmi, and F. Yu, “Three-Body Decays of Sleptons with General Flavor Violation and Left-Right Mixing,” *Phys.Rev.* **D79** (2009) 116009, arXiv:0904.1416 [hep-ph].
  - [25] J. L. Feng, S. T. French, I. Galon, C. G. Lester, Y. Nir, *et al.*, “Measuring Slepton Masses and Mixings at the LHC,” *JHEP* **1001** (2010) 047, arXiv:0910.1618 [hep-ph].
  - [26] A. De Simone, J. Fan, V. Sanz, and W. Skiba, “Leptogenic Supersymmetry,” *Phys. Rev.* **D80** (2009) 035010, arXiv:0903.5305 [hep-ph].
  - [27] J. L. Feng, S. T. French, C. G. Lester, Y. Nir, and Y. Shadmi, “The Shifted Peak: Resolving Nearly Degenerate Particles at the LHC,” *Phys.Rev.* **D80** (2009) 114004, arXiv:0906.4215 [hep-ph].
  - [28] T. Ito, R. Kitano, and T. Moroi, “Measurement of the Superparticle Mass Spectrum in the Long-Lived Stau Scenario at the LHC,” *JHEP* **1004** (2010) 017, arXiv:0910.5853 [hep-ph].
  - [29] R. Fok and G. D. Kribs, “mu to e in R-symmetric Supersymmetry,” *Phys.Rev.* **D82** (2010) 035010, arXiv:1004.0556 [hep-ph].
  - [30] A. Abada, A. J. R. Figueiredo, J. C. Romao, and A. M. Teixeira, “Interplay of LFV and slepton mass splittings at the LHC as a probe of the SUSY seesaw,” *JHEP* **10** (2010) 104, arXiv:1007.4833 [hep-ph].
  - [31] A. Abada, A. Figueiredo, J. Romao, and A. Teixeira, “Probing the supersymmetric type III seesaw: LFV at low-energies and at the LHC,” arXiv:1104.3962 [hep-ph].
  - [32] H. Dreiner, S. Grab, and T. Stefaniak, “Discovery Potential of Selectron or Smuon as the Lightest Supersymmetric Particle at the LHC,” arXiv:1102.3189 [hep-ph].
  - [33] B. Allanach, J. Conlon, and C. Lester, “Measuring Smuon-Selectron Mass Splitting at the CERN LHC and Patterns of Supersymmetry Breaking,” *Phys.Rev.* **D77** (2008) 076006, arXiv:0801.3666 [hep-ph].
  - [34] **The ATLAS Collaboration** Collaboration, G. Aad *et al.*, “Expected Performance of the ATLAS Experiment - Detector, Trigger and Physics,” arXiv:0901.0512 [hep-ex].
  - [35] “Search for squarks and gluinos using final states with jets and missing transverse momentum with the atlas detector in  $\sqrt{s} = 7\text{TeV}$  proton-proton collisions,” Tech. Rep. ATLAS-CONF-2011-086, CERN, Geneva, Jun, 2011.
  - [36] “Search for supersymmetry in all-hadronic events with  $\alpha_t$ ,” tech. rep., 2011.
  - [37] Y. Grossman, M. Martone, and D. J. Robinson, “Kinematic Edges with Flavor Oscillation and Non-Zero Widths,” arXiv:1108.5381 [hep-ph].
  - [38] **MEGA** Collaboration, M. L. Brooks *et al.*, “New Limit for the Family-Number Non-conserving Decay  $\mu^+ \rightarrow e^+ \gamma$ ,” *Phys. Rev. Lett.* **83** (1999) 1521–1524, arXiv:hep-ex/9905013.
  - [39] M. Ciuchini, A. Masiero, P. Paradisi, L. Silvestrini, S. Vempati, *et al.*, “Soft SUSY breaking grand unification: Leptons versus quarks on the flavor playground,” *Nucl.Phys.* **B783** (2007) 112–142, arXiv:hep-ph/0702144 [HEP-PH].
  - [40] F. Gabbiani, E. Gabrielli, A. Masiero, and L. Silvestrini, “A Complete analysis of FCNC and CP constraints in general SUSY extensions of the standard model,” *Nucl.Phys.* **B477** (1996) 321–352, arXiv:hep-ph/9604387 [hep-ph].
  - [41] G. Engelhard, J. L. Feng, I. Galon, D. Sanford, and F. Yu, “SPICE: Simulation Package for

- Including Flavor in Collider Events,” *Comput.Phys.Commun.* **181** (2010) 213–226, [arXiv:0904.1415 \[hep-ph\]](#).
- [42] B. Allanach, “SOFTSUSY: a program for calculating supersymmetric spectra,” *Comput.Phys.Commun.* **143** (2002) 305–331, [arXiv:hep-ph/0104145 \[hep-ph\]](#).
  - [43] A. Djouadi, M. Muhlleitner, and M. Spira, “Decays of supersymmetric particles: The Program SUSY-HIT (SUSpect-SdecaY-Hdecay-InTerface),” *Acta Phys.Polon.* **B38** (2007) 635–644, [arXiv:hep-ph/0609292 \[hep-ph\]](#).
  - [44] J. Alwall, P. Demin, S. de Visscher, R. Frederix, M. Herquet, *et al.*, “MadGraph/MadEvent v4: The New Web Generation,” *JHEP* **0709** (2007) 028, [arXiv:0706.2334 \[hep-ph\]](#).
  - [45] N. D. Christensen and C. Duhr, “FeynRules - Feynman rules made easy,” *Comput.Phys.Commun.* **180** (2009) 1614–1641, [arXiv:0806.4194 \[hep-ph\]](#).
  - [46] P. Meade and M. Reece, “BRIDGE: Branching ratio inquiry / decay generated events,” [arXiv:hep-ph/0703031 \[hep-ph\]](#).
  - [47] J. A. et. al, “MadGraph - Pythia Interface,” <http://madgraph.hep.uiuc.edu/> .
  - [48] T. Sjostrand, S. Mrenna, and P. Z. Skands, “PYTHIA 6.4 Physics and Manual,” *JHEP* **0605** (2006) 026, [arXiv:hep-ph/0603175 \[hep-ph\]](#).
  - [49] J. Conway, “PGS - Preaty Good Simulation ,” <http://www.physics.ucdavis.edu/~conway/research/software/pgs/pgs4-general.htm> .
  - [50] R. Brun and F. Rademakers, “ROOT: An object oriented data analysis framework,” *Nucl. Instrum. Meth.* **A389** (1997) 81–86.
  - [51] P. Demin, “ExROOT Analysis Package,” <http://madgraph.hep.uiuc.edu/> .
  - [52] J. M. Smillie and B. R. Webber, “Distinguishing Spins in Supersymmetric and Universal Extra Dimension Models at the Large Hadron Collider,” *JHEP* **10** (2005) 069, [arXiv:hep-ph/0507170](#).
  - [53] L.-T. Wang and I. Yavin, “A Review of Spin Determination at the LHC,” *Int. J. Mod. Phys.* **A23** (2008) 4647–4668, [arXiv:0802.2726 \[hep-ph\]](#).
  - [54] N. Arkani-Hamed, G. L. Kane, J. Thaler, and L.-T. Wang, “Supersymmetry and the LHC inverse problem,” *JHEP* **08** (2006) 070, [arXiv:hep-ph/0512190](#).